GCU
Glasgow Caledonian University

University for the Common Good

On PAPR reduction in pilot-assisted optical OFDM communication systems

Ogunkoya, Funmilayo B.; Sinanovic, Sinan; Popoola, Wasiu O.

Download date: 29. Apr. 2020

On PAPR Reduction in Pilot-Assisted Optical OFDM Communication Systems

Funmilayo B. Offiong, Sinan Sinanović and Wasiu O. Popoola

Abstract—**This paper presents a novel theoretical characterization of the pilot-assisted (PA) technique proposed for peak-to-average-power-ratio (PAPR) reduction in optical orthogonal frequency division multiplexing (O-OFDM). The two systems considered are direct-current biased O-OFDM (DCO-OFDM) and asymmetrically clipped O-OFDM (ACO-OFDM) in optical wireless communications. The DCO-OFDM and ACO-OFDM time domain signals approach Gaussian and half-Gaussian distributions respectively. The PA technique uses P iterations of a pilot sequence to rotate the phase of U data symbols within a PA O-OFDM frame and select the frame with the least PAPR. Thus, we utilize order statistics to characterize the PAPR distributions of the PA DCO-OFDM and ACO-OFDM system. The PA technique results in higher reduction in PAPR for high P but at the expense of increased complexity. In the theoretical framework developed, we are able to determine P that gives reasonable PAPR reduction gain. The theoretical analysis of PAPR reduction effects on the average optical and electrical signal power is studied. Results show that the PA technique is capable of reducing the optical energy per bit to noise power spectral density $E_{b(opt)}/N_0$ ratio required to meet target bit-error-rate (BER) in an additive white Gaussian noise (AWGN) channel. Comparisons of the analytical results of PA O-OFDM signal with that of computer simulations show very good agreement.**

Index Terms—**Optical OFDM; pilot-assisted PAPR reduction analysis; DCO-OFDM and ACO-OFDM PAPR distributions; order statistics.**

I. INTRODUCTION

THE wireless communication data traffic is growing exponentially with the increasing popularity of smart devices, data-intensive applications and services [1]. Optical wireless communications (OWC) is a promising alternative technology with significantly large and unregulated spectrum to complement the existing radio frequency (RF) communication systems. The dynamic range and bandwidth limitations in the front-end devices and impairments in the channel of the OWC system prevent full exploitation of the huge optical spectrum in achieving high-speed communications. To fully leverage the inherent resources of OWC and mitigate the effects of these limitations, a multi-carrier modulation technique such as optical orthogonal frequency division multiplexing (O-OFDM) is an attractive option [2]. However, implementing O-OFDM in OWC systems has the problem of the high peak-to-average power ratio (PAPR) due to the constraints on the average

radiated optical power and the limited dynamic range of the front-end devices [3]. Hence, effort to mitigate high PAPR problem in O-OFDM is very important in order to have optimum system performance, power efficiency and optimal utilization of the available optical spectrum.

The limited dynamic range of the light emitting diodes (LEDs) poses constraints on the O-OFDM signal [4]. This means that the full amplitude swing of the O-OFDM signal with high peaks will not fit within the limited range without being clipped. Signal clipping causes degradation in the error performance of the system. As such, optimal conditioning of the O-OFDM signal becomes crucial in order to become suitable for transmission through the LED and other front-end devices. There have been a number of studies in literature proposing different solutions to address the high peak values and average optical power in O-OFDM. These techniques include the use of branch and bound method in tone injection scheme to reduce the peaks of the electrical signal [5]. In another approach reported in [6], the O-OFDM signal is modulated onto an ellipse to reduce the PAPR of the signal. The PAPR reduction capability and error performance of the ellipse-based approach greatly depend on the ratio of the major to minor radius of the ellipse. The generation of series of Toeplitz matrix using the time domain signal out of which the signal with the lowest PAPR is selected for transmission has equally been investigated in [7]. While this matrix-based Gaussian blur method provides PAPR reduction, it however sacrifices the error rate of the system due to the signal recovery error at the receiver. Technique in [8] achieves electrical PAPR reduction by embedding pilot signal within the O-OFDM signal in the frequency domain in order to obtain the time domain signal with reduced PAPR value. The work presented in this paper is the theoretical evaluation of the pilot-assisted (PA) PAPR reduction technique presented in [8]. A detailed survey and description of PAPR reduction techniques in OFDM can be found in [9].

It is equally important to mention that besides the PAPR, there are other metrics like cubic metric (CM) [10], instantaneous-to-average power ratio (IAPR) [11], and peak-to-mean envelope power ratio (PMEPR) [12] used to measure envelop fluctuations but PAPR is the most widely used. The statistical distribution of PAPR focuses on the maximum peak in the envelop variation of an O-OFDM symbol. The complementary cumulative distribution function (CCDF) has been widely used in the literature as a metric to characterize the PAPR reduction capability of various techniques [9] (and references therein). The complex-valued bipolar time domain OFDM signal is used in RF systems while the OWC system

F. B. Offiong is with the Department of Electronic and Electrical Engineering, Obafemi Awolowo University, Ile-Ife, 220005, Nigeria, (email: fboffiong@ieee.org). S. Sinanović is with the School of Engineering and Built Environment, Glasgow Caledonian University, Glasgow, G4 0BA, UK, (email: sinan.sinanovic@gcu.ac.uk). W. O. Popoola is with the Institute for Digital Communications, University of Edinburgh, Edinburgh, EH9 3JL, UK, (email: W.Popoola@ed.ac.uk).

uses the real-valued unipolar time domain O-OFDM signal [13]. Furthermore, the RF system is limited by the average electrical power and peak power while the OWC system constraints are average optical power and dynamic optical power [14]. Thus, some of the PAPR reduction techniques in an RF system and its theoretical frameworks cannot be directly applied to the OWC system. There has been intensive research effort to analyze the PAPR distributions of complex-valued OFDM signals, and in techniques to reduce the PAPR [15], [16]. It is equally noted that the PAPR distributions of the real-valued O-OFDM signal without PAPR reduction techniques have been presented in the literature [17], [18]. However, there is little reported work in the open literature on the theoretical analysis of the distributions of PAPR in O-OFDM systems with PAPR reduction techniques. Analysis of the electrical PAPR distributions will provide a guideline for practical implementation of the techniques. Moreover, PAPR is one of the most important parameters of interest used in specifying the dynamic range of the digital-to-analog converter (DAC) in an OFDM system [15]. O-OFDM signal peaks reduction provides the opportunity of implementing power-efficient LED drivers in OWC system. Thus, theoretical characterization of the PAPR distributions is important.

In the PA technique [8], the electrical PAPR reduction is achieved by rotating the phase of clusters of data symbols within a frame with P iterations of a randomly generated pilot symbol sequence with specially chosen phase and amplitude following the initial principles found in [19] and [20]. The phase rotation reduces the probability of having subcarriers adding up coherently to produce high peaks in the time domain. Thus, the time domain PA O-OFDM frame with the least PAPR after P iterations is selected for transmission. Pilot symbol recovery at the receiver is done using the maximum likelihood (ML) estimation scheme. In PAPR reduction technique via non-recoverable signal clipping, there is the possibility of attaining any desired level of PAPR reduction but at the expense of degrading the bit-error-rate (BER) performance of the system [8]. However, the PA technique does not only offer good PAPR reduction capability, but it does so without introducing error performance degradation. The number of P iterations used for data phase rotation depends on the magnitude of the PAPR reduction desirable but at the expense of increased computational complexity. However, recent advances in solid-state technology make it possible to implement the technique in a fast and cost-effective manner. The empirical evaluation of the PA technique in real indoor OWC channel with the possibility of using the transmitted pilot symbol for channel estimation at the receiver is studied in [21]. While PA technique for PAPR reduction in O-OFDM was investigated via computer simulations in [8], a theoretical analysis for the scheme was not presented. Also, the need for multiple transmit chains poses a major challenge in spatial domain O-OFDM system utilizing grouped LEDs [22]–[24]. Thus, the study in [25] proposed the use of PA technique to limit the number of transmit chains in the system and further reduce PAPR.

This paper presents a theoretical characterization of the PA technique proposed for PAPR reduction in O-OFDM using order statistics. In this work, we apply order statistics in the field of OWC for the first time to predict the distributions of the PAPR of PA O-OFDM signal. Our contributions include 1) analytical framework of the electrical PAPR distribution of the PA direct-current biased O-OFDM (DCO-OFDM); 2) required DC bias to make the PA DCO-OFDM signal unipolar; 3) the derivation of the PAPR distributions of PA asymmetrically clipped O-OFDM (ACO-OFDM) signal; and 4) investigation of the average optical power reduction gain by implementing the PA technique in O-OFDM. The PAPR reduction is characterized by considering the CCDF metric in accordance with the general way of presenting results on the subject [9]. Comparisons of the PA O-OFDM system, to obtain their PAPR reduction capability, are made with basic O-OFDM where no PAPR reduction technique is implemented. The error performance is assessed in terms of the optical and electrical energy per bit to noise power spectral density ratio required to meet target BER. The theoretical results of the PA O-OFDM are compared with simulation results in order to confirm the accuracy of the analysis.

The rest of the paper is outlined as follows: a brief description of basic O-OFDM is presented in Section II. A concise review of the PA technique in O-OFDM is presented in Section III. Section IV-A and IV-B gives a brief overview of order statistics and the procedure of selecting the PA frame with the least PAPR after P iterations respectively. The theoretical framework of PAPR distributions of the PA technique in DCO-OFDM system is presented in Section IV-C. The closed form solution of the PAPR distributions of basic ACO-OFDM and PA ACO-OFDM is presented in Section IV-D. Error performance of the PA technique in DCO-OFDM and ACO-OFDM is studied in Section V. Results with relevant discussions are contained in Section VI. Finally, Section VII concludes the paper.

II. OFDM-Based Optical Communication Systems

Most of the practical OWC systems currently in use are based on the scheme called intensity modulation with direct detection (IM/DD) [3]. This requires the modulating signal to be real and non-negative for the purpose of transmission on light intensity which is positive-valued [26]. The real-valued signal is obtained in O-OFDM by constraining the frequency domain data-carrying inverse fast Fourier transform (IFFT) subcarriers to have Hermitian symmetry [27]. Hermitian symmetry ensures real O-OFDM signal which is still bipolar. Hence, a number of approaches to generate unipolar signal have been proposed. These include DCO-OFDM [28], ACO-OFDM [29], pulse-amplitude-modulated discrete multitone modulation (PAM-DMT) [30] and other modified version of the listed O-OFDM variants [31], [32]. A complex-valued polar OFDM (P-OFDM) has been proposed in [33] for optical communication systems. The major difference in the implementation of O-OFDM variants is in the format of mapping data symbols to the IFFT subcarriers and the bipolar-to-unipolar conversion process of the time domain signal. In comparison with other O-OFDM based schemes, DCO-OFDM requires the addition of DC bias which results in power penalty

[31]. However, addition of some DC bias to the O-OFDM signal is essential for visible light communication (VLC) applications where illumination is the primary purpose of the optical source. The non-negative signal generation process for ACO-OFDM and PAM-DMT sacrifices half of the spectral efficiency when compared with DCO-OFDM.

In a basic O-OFDM based wireless communication system, data stream converted from serial to parallel is mapped to block of symbols from a digital modulation scheme such as M-ary quadrature amplitude modulation (M-QAM) or pulse amplitude modulation (M-PAM). Hermitian symmetry is imposed on the block of symbols to ensure real-valued bipolar time domain signal. Thereafter, O-OFDM symbol is accomplished by mapping the resulting Hermitian symmetric M-ary block of symbols to IFFT subcarriers [28]. The IFFT operation generates real-valued bipolar time domain O-OFDM symbol. The superposition of the subcarriers results in occasional high peaks in the time domain signal. The bipolar O-OFDM symbol is converted to unipolar based on the O-OFDM scheme in use. Cyclic prefix (CP) is utilized to make the O-OFDM symbol robust to inter-symbol interference (ISI) [27]. Addition of CP to the O-OFDM symbol facilitates the implementation of simplified single-tap equalization technique at the receiver. Thereafter, the discrete real-valued unipolar O-OFDM symbol samples are passed through DAC and filtered to generate a continuous time domain O-OFDM signal. This electrical baseband signal is then fed into the LED driver to modulate the intensity of the LED at the transmitter. Thereafter, the LED converts the electrical signal to optical signal and radiates the information-bearing optical signal through free space. At the receiver, a photodetector converts the incoming optical signal into an electrical current signal. The transimpedance amplifier (TIA) turns this current signal into a voltage signal suitable for a post detection amplifier to boost to an appropriate level suitable for an analog-to-digital converter (ADC) to act upon for further processing. Estimates of the transmitted data stream is recovered through a reverse operation of the processes performed at the transmitter.

III. PAPR REDUCTION IN O-OFDM USING THE PA TECHNIQUE

In this section, we present an overview of the PA PAPR reduction technique in DCO-OFDM and ACO-OFDM.

A. Review of the PA Technique for PAPR Reduction in DCO-OFDM

The block diagram of the O-OFDM system using the PA technique for PAPR reduction is illustrated in Fig. 1. The system consists of randomly generated data streams, $\mathbf{X}_d$, mapped to an M-QAM constellation. The M-QAM data symbols are grouped into cluster of U data symbols to form $\mathbf{X}_s^u$, $u = 1, 2, \ldots, U$. Thereafter, a randomly generated pilot symbol sequence, $\mathbf{X}_p$, is combined with $\mathbf{X}_s^u$ to form a PA O-OFDM frame. Each of the cluster of $U + 1$ symbols in the PA O-OFDM frame has n_s active subcarriers. The phase of the pilot symbol represented as θ_{ip}; $i = 1, 2, \ldots, n_s$; $p = 1, 2, \ldots, P$, is used to rotate the phase of the data symbols

θ_{iu}; $i = 1, 2, \ldots$; $n_s, u = 1, 2, \ldots, U$, to obtain signal $\mathbf{X}_{sp}$ as described in (1):

$$
\mathbf{X}_{sp} = \begin{pmatrix}
a_{11}\underline{/\theta_{11} + \theta_{1p}} & \cdots & a_{1u}\underline{/\theta_{1u} + \theta_{1p}} & \cdots & a_{1U}\underline{/\theta_{1U} + \theta_{1p}} & 1\underline{/\theta_{1p}} \\
a_{21}\underline{/\theta_{21} + \theta_{2p}} & \cdots & a_{2u}\underline{/\theta_{2u} + \theta_{2p}} & \cdots & a_{2U}\underline{/\theta_{2U} + \theta_{2p}} & 1\underline{/\theta_{2p}} \\
\vdots & \vdots & \vdots & \vdots & \vdots & \vdots \\
a_{i1}\underline{/\theta_{i1} + \theta_{ip}} & \cdots & a_{iu}\underline{/\theta_{iu} + \theta_{ip}} & \cdots & a_{iU}\underline{/\theta_{iU} + \theta_{ip}} & 1\underline{/\theta_{ip}} \\
\vdots & \vdots & \vdots & \vdots & \vdots & \vdots \\
a_{n_s1}\underline{/\theta_{n_s1} + \theta_{n_sp}} & \cdots & a_{n_su}\underline{/\theta_{n_su} + \theta_{n_sp}} & \cdots & a_{n_sU}\underline{/\theta_{n_sU} + \theta_{n_sp}} & 1\underline{/\theta_{n_sp}}
\end{pmatrix}
\tag{1}
$$

where a_{iu} and θ_{iu} are the QAM constellation amplitude and phase of the ith subcarrier and u^{th} symbol respectively, while θ_{ip} is the phase of the ith subcarrier of the pth pilot symbol sequence. The pilot symbol amplitude is constrained to unity in order to preserve the electrical power of the data signals, while its phase θ_{ip} can either be 0 or π so as to maintain original constellation of the input data symbols. This choice of pilot phase also eases the signal recovery at the receiver [8].

To obtain a real-valued time domain signal, Hermitian symmetry is imposed on the uth symbol, $\mathbf{X}_{sp}^u(i)$, in the frame to obtain signal $\mathbf{X}^u(i)$, $i = 0, 1, \ldots, NL - 1$. The Hermitian symmetry operation increases the number of subcarriers per symbol from n_s to $N = 2(1 + n_s)$. Symbol $\mathbf{X}^u(i)$ also contains $N(L - 1)$ padding zeros to account for L-times oversampling required to adequately capture the signal peaks. The Hermitian symmetry operation requires that the mirror of the complex conjugate of the subcarriers is appended. This is mathematically described with the uth symbol as in (2):

$$
\mathbf{X}^u = \left[0, \mathbf{X}_{sp}^u(i), \underbrace{0, 0, \ldots, 0}_{N(L-1)/2}, 0, \underbrace{0, 0, \ldots, 0}_{N(L-1)/2}, \mathbf{X}_{sp}^{u*}(NL - i) \right]^{\text{T}},
\tag{2}
$$

where $[X]^{\text{T}}$ is the transpose of X and $X^*(\cdot)$ denotes complex conjugate of $X(\cdot)$. The PA O-OFDM frame $\mathbf{X}^u$ is input to the IFFT of NL sampling points. The IFFT operation generates the real-valued discrete time domain signal $x(n)$. Signal $x(n)$ is converted from parallel-to-serial followed by addition of CP and DAC to obtain the continuous time domain signal $x_{\text{dc}}(t)$.

The process of rotating the phase of the data symbols, $\mathbf{X}_s^u$, with phase of pilot symbol, $\mathbf{X}_p$, is repeated with another random sequence of pilot symbols up to P times. This results in a P randomly generated pilot symbol sequence, $\mathbf{X}_p$, $p = 1, 2, \ldots, P$. Thus, the PAPR reduction is achieved by selecting the pilot symbol sequence that avoids coherent addition of the subcarriers $\mathbf{X}^u(i)$ as much as possible [8]. This corresponds to the PA O-OFDM frame with the lowest PAPR. The electrical PAPR of an oversampled PA O-OFDM frame after P iterations is given as [8]:

$$
\text{PAPR}\{x(n)\} = \underset{1 \leq p \leq P}{\arg\min}\{\text{PAPR}_p\{x(n)\}\}
$$

$$
= \underset{1 \leq p \leq P}{\arg\min} \left[\frac{\underset{0 \leq n \leq (U+1)(NL-1)}{\max} |x(n)|^2}{\sigma_x^2} \right].
\tag{3}
$$

where $\sigma_x^2 = \text{E}[|x(n)|^2]$ and $\text{E}[\cdot]$ denotes the statistical expectation. The CCDF of $\text{PAPR}\{x(n)\}$, $\text{P}(y)$, is expressed as:

$$
\text{P}(y) = \text{Pr}\left(\text{PAPR}\{x(n)\} \geq y\right),
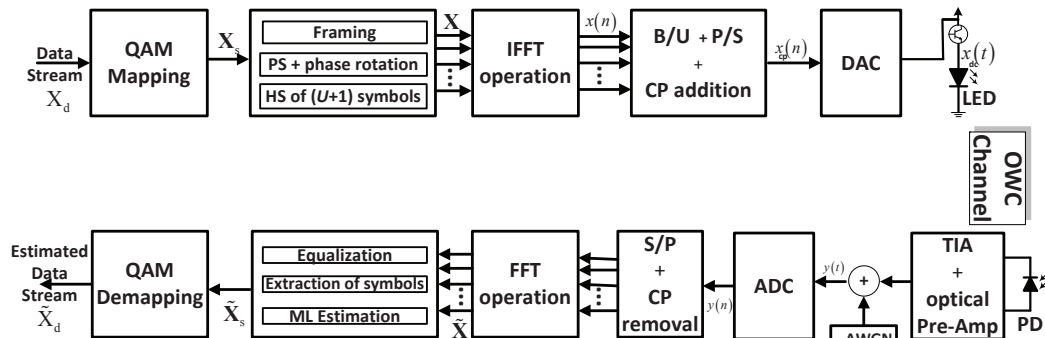\tag{4}
$$

Fig. 1: Block diagram illustrating the pilot-assisted O-OFDM system. PS: pilot symbol, HS: Hermitian symmetry, B/U: Bipolar-to-unipolar, P/S: Parallel-to-serial, TIA: Transimpedance amplifier S/P:serial-to-parallel

where P is the probability of PAPR$\{x(n)\}$ exceeding a threshold value of y.

The spectral efficiency, η_{DCO}, of the PA DCO-OFDM frame is expressed as:

$$\eta_{\text{DCO}} = \frac{(\log_2 M)(n_s U)}{2(n_s + 1)(U + 1)} \quad \text{bits/s/Hz}, \quad (5)$$

where the term $\log_2 M$ denotes the number of encoded bits per M-QAM constellation point.

The received signal, in the frequency domain, is given by:

$$\mathbf{Y}^u(i) = \mathbf{H}(i)\mathbf{X}^u(i) + \mathbf{W}(i);$$
$$u = 1, 2, \ldots, U + 1; \quad i = 0, 1, \ldots, NL - 1, \quad (6)$$

where $\mathbf{H}(i)$ is the channel's frequency response for the ith subcarrier. The receiver noise is assumed to be ambient induced shot noise and is modeled as additive white Gaussia noise (AWGN). A simplified most widely used single-tap equalization technique like zero-forcing (ZF) can be utilized to obtain signal $\tilde{X}^u(i)$ as [8]:

$$\tilde{X}^u(i) = \frac{Y^u(i)}{H(i)}. \quad (7)$$

Removal of Hermitian symmetric symbols imposed at the transmitter from the signal $\tilde{X}^u(i)$ gives signal $\tilde{X}^u_{\text{sp}}(i)$; $i = 1, 2, \ldots, n_s$.

The constraint on the amplitude and phase of the pilot symbol sequence at the transmitter results in $\mathbf{X}_p(i) \in \{\pm 1\}$ for $i = 1, 2, \ldots, n_s$. This makes the ML estimation technique suitable at the receiver [8] as it helps to minimize the number of combinations needed to be searched in estimating the pilot symbol sequence. Based on the ML decision rule, the transmitted pilot symbol sequence, $\mathbf{X}_p(i)$, is estimated at the receiver as:

$$\hat{\mathbf{X}}_p(i) = \begin{cases} +1 & \text{if } \Re\{\tilde{\mathbf{X}}^{U+1}_{\text{sp}}(i)\} \geq 0 \\ -1 & \text{otherwise} \end{cases} \quad (8)$$

where $\Re\{\cdot\}$ represents the real part. Thus, the data symbol can be recovered from (9) as:

$$\tilde{\mathbf{X}}^u_s(i) = \frac{\tilde{\mathbf{X}}^u_{\text{sp}}(i)}{\hat{\mathbf{X}}_p(i)}; \quad u = 1, 2, \ldots, U. \quad (9)$$

Finally, $\tilde{X}^u_s(i)$ is mapped onto the quadrature amplitude de-modulator to obtain estimates of the transmitted data stream.

B. PA Technique for PAPR Reduction in ACO-OFDM

The ACO-OFDM system involves activating the odd sub-carriers of the IFFT. The Hermitian symmetry has to be satisfied in order to obtain real-valued time domain signal at the output of IFFT. Thus, the same procedure of M-QAM data symbols phase rotation with P iterations of pilot symbol sequence as described in the case of DCO-OFDM is followed. The cluster of $U + 1$ symbols are loaded onto odd subcarriers only while even subcarriers are set to zero as presented in [29]. If $X_s(i)$ with $i = 0, 1, \ldots, n_s$ represent the M-QAM constellation symbols, then the input to the IFFT $\mathbf{X}^u_{\text{ACO}}$, $u = 1, 2, \ldots, U + 1$ is illustrated with the uth symbol as:

$$\mathbf{X}^u_{\text{aco}} = [0, X_s(i), 0, X_s(i+1), \ldots, 0, X_s(n_s-1), 0,$$
$$X_s(n_s), \underbrace{0, 0, \ldots, 0}_{N(L-1)/2}, 0, \underbrace{0, 0, \ldots, 0}_{N(L-1)/2}, X_s^*(n_s),$$
$$0, X_s^*(n_s-1), \ldots, X_s^*(i+1), 0, X_s^*(i)]^{\text{T}}, \quad (10)$$

For n_s active data subcarriers, the total number of frequency domain subcarriers utilized in ACO-OFDM after Hermitian symmetry increases to $N = 4n_s$. ACO-OFDM exploit the properties of Hermitian symmetry and Fourier transform to achieve nonnegativity without any loss of information. This is done at the expense of reduced spectral efficiency as a result of modulating odd subcarriers only. Since all even subcarriers in frequency domain are zero, symmetry property discussed in [29] produces pair of time domain samples, $x(n)$, with

the same magnitude but opposite signs. Mathematically, the bipolar discrete time domain samples $x(n)$ is obtained as:

$$
\begin{aligned}
x(n) &= \mathrm{IFFT}[\mathbf{X}_{\mathrm{aco}}], & 0 \leq n \leq NL - 1, \\
&= -x(n + NL/2), & 0 \leq n \leq NL/2 - 1.
\end{aligned}
\tag{11}
$$

The negative part of the time domain samples is clipped at zero-level to obtain unipolar ACO-OFDM signal, $x_{\mathrm{aco}}(n)$, given by (12). For every pair of samples, the clipped negative samples still have the same information contained in the positive samples.

$$
x_{\mathrm{aco}}(n) = \begin{cases} x(n), & x(n) \geq 0, & 0 \leq n \leq NL - 1 \\ 0, & \text{otherwise} \end{cases}
\tag{12}
$$

After default clipping of all negative samples in ACO-OFDM, the distribution of $x_{\mathrm{aco}}(n)$ converge to a half-normal distribution for $x_{\mathrm{aco}}(n) > 0$. The asymmetric clipping advantageously reduces the number of samples and the electrical average power by half, that is, $\mathrm{E}\{x_{\mathrm{aco}}^2(n)\} = \sigma_x^2/2$. Hence, the remaining upper PAPR of ACO-OFDM signal can be defined as:

$$
\mathrm{PAPR_A} \triangleq \frac{\displaystyle\max_{0 \leq n \leq NL-1} x_{\mathrm{aco}}^2(n)}{\sigma_x^2/2}
\tag{13}
$$

For a PA ACO-OFDM frame, the spectral efficiency, η_{ACO}, is obtained as:

$$
\eta_{\mathrm{aco}} = \frac{(\log_2 M)U}{4(U + 1)} \quad \text{bits/s/Hz.}
\tag{14}
$$

IV. THEORETICAL ANALYSIS OF THE PAPR DISTRIBUTIONS OF PA O-OFDM SIGNAL

In this section, we present the theoretical analysis of the PAPR distributions of the PA DCO-OFDM and ACO-OFDM signals using order statistics [34] and the approximate cumulative distribution function (CDF) of a basic O-OFDM symbol. The derivations of DCO-OFDM and ACO-OFDM PAPR distributions are based on the assumption that the time domain signal follows a perfect Gaussian and half-Gaussian distribution respectively. The M-QAM symbols are normalized for unity average electrical power.

A. Order Statistics

Order statistics is a branch of statistics which is among the fundamental tools used in non-parametric and inference evaluations [34], [35]. Order statistic seeks to assess the statistics of a given ordered samples of random variables. It has important special cases which include minimum and maximum order statistics. These cases can also be referred to as extreme order statistics in some cases. Order statistics were first applied to real signal processing problems in the 1900s [36]. Over the years, application of order statistics as an analytical tool has continued to expand to diverse disciplines and fields which include RF wireless communications [35]. Order statistics have been applied in channel adaptation scheme which is an essential concept in wireless communication to achieve highly spectral and power efficient transmission over fading channel condition [35].

In order to further explore the potential of order statistics in advanced wireless communications, we apply order statistics in the field of OWC for the first time using the distribution functions of the maximum and minimum order statistics. These distribution functions of maximum and minimum order statistics are utilized to characterize the PAPR of the PA O-OFDM signal. With the knowledge of the PAPR distribution of an O-OFDM symbol, we utilized maximum order statistics to characterize the PAPR distributions of the PA O-OFDM frame. Thereafter, we applied minimum order statistics to the derived distributions of the PA O-OFDM frames to select the frame with the minimum PAPR after P-iterations of data symbols phase rotation.

Independent and identically distributed (i.i.d.) continuous random variables $Y_1, Y_2, \ldots, Y_k, \ldots, Y_q$ denote an ensemble observed at instants $k = 1, 2, 3, \ldots, q$ respectively. The order statistics is focused on $Y_{(1)}, Y_{(2)}, \ldots, Y_{(k)}, \ldots, Y_{(q)}$, where $Y_{(1)} \leq Y_{(2)} \leq \ldots \leq Y_{(k)} \leq \ldots \leq Y_{(q)}$ and subscript (k) denotes the kth order statistics [34].

If Y_k has probability distribution function (PDF), $f_Y(y)$, and CDF, $F_Y(y)$, then the PDF of the kth order statistics is given by [34]:

$$
f_{Y_{(k)}}(y) = \frac{q!}{(k-1)!(q-k)!} [F_Y(y)]^{k-1} [1 - F_Y(y)]^{q-k} f_Y(y).
\tag{15}
$$

Consequently, the PDF of the maximum order statistics, $Y_{(q)}$, can be obtained from (15) as:

$$
f_{Y_{(q)}}(y) = q [F_Y(y)]^{q-1} \frac{\mathrm{d}}{\mathrm{d}y} F_Y(y).
\tag{16}
$$

Likewise, the PDF of the minimum order statistics, $Y_{(1)}$, can also be obtained from (15) as:

$$
\begin{aligned}
f_{Y_{(1)}}(y) &= q [1 - F_Y(y)]^{q-1} f_Y(y) \\
&= q [1 - F_Y(y)]^{q-1} \frac{\mathrm{d}}{\mathrm{d}y} F_Y(y).
\end{aligned}
\tag{17}
$$

The integral of (17) gives the CDF of the minimum order as:

$$
F_{Y_{(1)}}(y) = \int_{-\infty}^{y} f_{Y_{(1)}}(t) \, \mathrm{d}t.
\tag{18}
$$

Hence, the CCDF of the minimum order statistics can be evaluated from (18) as: $1 - F_{Y_{(1)}}(y)$.

B. Procedure of Analyzing the Distributions of the PA O-OFDM Frame with the Least PAPR

The PA O-OFDM frame has $U + 1$ O-OFDM symbols, with each of the symbols having NL samples in the discrete time domain. The iterations in the PA technique results in P of PA O-OFDM frames out of which the one with the minimum PAPR is selected. Thus, to analyze the CCDF of PAPR of the PA O-OFDM frame, the procedure used is summarized as follows:

- The CDF of the $U + 1$ O-OFDM symbols in a PA frame is obtained.
- The PDF of the O-OFDM symbol with the highest peak within a frame is derived by employing maximum order statistics on the CDF of the $U + 1$ O-OFDM symbols.

- The integral of this PDF follows to obtain the CDF of a PA O-OFDM frame.
- PA technique involves selection of the PA O-OFDM frame with least PAPR after P iterations. Thus, minimum order statistics is used to the obtain PDF of the PA O-OFDM frame with the least PAPR.
- Thereafter, an integral of the resulting PDF follows to obtain the CDF of the PA O-OFDM with PAPR reduction. Finally, the corresponding CCDF of PAPR of the PA O-OFDM frame with PAPR reduction is obtained from the CDF.

C. Signal Distribution of the O-OFDM Frame

The DCO-OFDM PAPR distributions are presented in this Section. For the DCO-OFDM derivations, we shall use the term basic O-OFDM and PA O-OFDM to indicate bipolar DCO-OFDM signal prior to the addition of DC bias to achieve required unipolar signal. The CDF of PAPR of real-valued basic O-OFDM symbol can be shown to be [17]:

$$F_Y(y) = (1 - 2Q(\sqrt{y}))^{\alpha N} \qquad (19)$$

where $Q(x) = \frac{1}{\sqrt{2\pi}} \int_x^\infty e^{-u^2/2} \, du$ represents the Q-function and α is an empirical factor. Equation (19) represents the CDF of each symbol in the PA O-OFDM frame. This equation is based on the assumption that the IFFT output samples approach Gaussian random variables as N increases. As mentioned earlier, oversampling of discrete O-OFDM signal is done in order to accurately model a continuous time domain signal and fully capture the signal highest peak. The PAPR of the $L = 4$ times oversampled discrete signal has been established to accurately approximate that of a continuous time domain OFDM signal [37]. L-times oversampling in O-OFDM is done with the addition of padding zeros in the frequency domain and this leads to an increase in the IFFT sampling points from N to NL. As a result, the distribution of the L-times oversampled time domain signal deviates from being sum of NL independent variables depending on size of L. This deviation is adjusted by approximating the distribution of the PAPR of L-times oversampled signal by αN-length Gaussian random variables. α is an empirical factor and without loss of generality we chose $\alpha = 2.8$ in this work, based on [38], [39].

1) Signal distribution of the O-OFDM frame with PA PAPR reduction: The CDF of the PA frame before PAPR reduction can be obtained using maximum order statistics with the notion that the distribution contains $U + 1$ symbols in a PA O-OFDM frame. The pilot symbol is also included in the evaluation of the electrical PAPR since it is transmitted alongside the data symbols. The CP is omitted in the derivations for simplicity since it does not introduce new peaks in the O-OFDM signal. Thus, the CDF of a PA O-OFDM frame is obtained as (see proof in Appendix A):

$$F_{Y_{(U_p)}}(y) = (1 - 2Q(\sqrt{y}))^{\alpha N U_p}. \qquad (20)$$

where $U_p = U + 1$ represents the size of the PA O-OFDM frame containing U data symbols and one pilot symbol.

To analyze the PA O-OFDM frame that gives the minimum PAPR after rotating the phase of the U symbols with P pilot symbol sequences, we use order statistics again. Here the ensemble consists of P PAPR distributions each with a CDF given by (20). The distribution of minimum PAPR out of P iterations is obtained by finding the minimum order statistics. Using (20), we obtain the PDF of the minimum PAPR as:

$$f_{Y_{m(1)}}(y) = P\left[1 - (1 - 2Q(\sqrt{y}))^{\alpha N U_p}\right]^{P-1} \times$$
$$\left[\frac{\alpha N U_p}{\sqrt{2\pi y}} e^{-y/2} (1 - 2Q(\sqrt{y}))^{\alpha N U_p - 1}\right]. \qquad (21)$$

The corresponding CDF can be obtained by taking the integral of (21). Since PAPR value is always positive, this gives:

$$F_{Y_{m(1)}}(y) = 1 - \left[1 - (1 - 2Q(\sqrt{y}))^{\alpha N U_p}\right]^P. \qquad (22)$$

See Appendix B for the proof of (22). The CCDF of PAPR of the oversampled PA O-OFDM bipolar signal $x(n)$ is thus:

$$P_d(y) = \left[1 - (1 - 2Q(\sqrt{y}))^{\alpha N U_p}\right]^P. \qquad (23)$$

2) Alternative approach of deriving the signal distribution of the O-OFDM frame with PA PAPR reduction: Equation (23) uses the PAPR distribution of the oversampled discrete time domain O-OFDM signal. Also, based on the assumption of Guassian distribution of the time domain signal, the CDF of PAPR of the real-valued continuous time O-OFDM signal can be shown to be [17]:

$$F_Y(y_c) = e^{-\frac{N e^{-y_c/2}}{\sqrt{3}}}. \qquad (24)$$

Using (24) and the same summarized procedure of order statistics in Section IV-B, the CCDF of PAPR of the continuous time domain PA O-OFDM signal is obtained as:

$$P_c(y_c) = \left(1 - e^{-\frac{U_p N e^{-y_c/2}}{\sqrt{3}}}\right)^P. \qquad (25)$$

Equations (23) and (25) are the analytical distributions of PAPR of the PA O-OFDM derived using two different expressions of CDF of a basic O-OFDM symbol. Fig. 2 shows the CCDF plot of the PAPR of basic and PA O-OFDM signals. The accuracy of the derived expressions for CCDF of PAPR from (23) and (25) are verified and compared with simulations presented in this figure. For this purpose, a data-carrying IFFT size of $N = [256, 1024]$ and oversampling factor of $L = 4$ are chosen. Analysis based on (23) and (25) are independent of M-QAM since $E[|X(i)|^2] = 1$ for all QAM systems. Comparing the CCDF of PA O-OFDM when $N = 256$, results show a near-perfect agreement between those obtained using (23) when $\alpha = 2.8$ and (25). However, there is a difference in PAPR levels of about 0.1 dB between analysis and simulation. This is because the analysis assume perfect Gaussian distribution of the O-OFDM signal while simulations only approach Gaussianity as N increases. As the number of subcarriers increases from $N = 256$ to $N = 1024$, the central limit theorem holds better since simulated results show better match with analytical results. PAPR reduction gain is quantified by comparing the basic O-OFDM signal with the PA O-OFDM signal. At CCDF $= 10^{-3}$, the PAPR reduction using $P = 5$ and $N = 1024$ is about 2.1 dB. Greater reduction in PAPR can be achieved at lower CCDF.
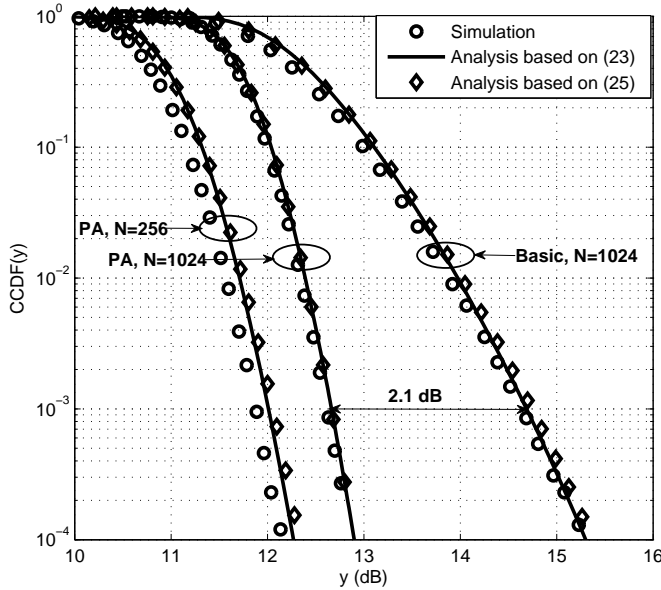
Fig. 2: CCDF plot for basic and PA O-OFDM signal using $P = 5$, $U = 5$, $n_s = [127, 511]$ and $N = [256, 1024]$.

3) Signal distribution of the DCO-OFDM frame with PA PAPR reduction: The theoretical analysis of the required DC bias in the DCO-OFDM signal and the resulting PAPR distributions of the PA DCO-OFDM signal are presented here. Addition of DC bias, $\mathcal{B}$, to obtain unipolar signal, $x_{dc}(t)$, needed to drive the optical modulator results in:

$$x_{dc}(t) = x(t) + \mathcal{B}, \tag{26}$$

In (26) it is assuming a linear driver and an ideal intensity modulator. The zero-mean signal, $x(t)$, has a variance of $\sigma_x^2 = P_{s(elect)}$, where $P_{s(elect)}$ is the average electrical symbol power. $\mathcal{B}$ is usually set relative to the standard deviation, σ_x, of $x(t)$ [28], i.e $\mathcal{B} = \mathcal{K}\sigma_x$, where $\mathcal{K}$ is a constant representing the normalized DC bias level. The unipolar signal to be transmitted, $x_{dc}(t)$, also has a Gaussian distribution with mean of $\mathcal{B} = P_{s(opt)}$, where $P_{s(opt)}$ is the average optical symbol power when clipping is minimal.

Thus, using (23) we obtain the CCDF of the PAPR of the oversampled PA DCO-OFDM signal as:

$$P_{d_{dc}}(y) = Pr \left[\underset{1 \leq p \leq P}{\arg\min} \left(\frac{\underset{0 \leq n \leq U_p(NL-1)}{\max}(x_{dc}(n))^2}{E[(x_{dc}(n))^2]} \right) > y \right]$$

$$= \left[1 - \left(1 - 2Q(\sqrt{y(1+\mathcal{K}^2)} - \mathcal{K}) \right)^{\alpha NU_p} \right]^P, \tag{27}$$

where $E\{x_{dc}^2\} = \sigma_x^2 + \mathcal{B}^2$ is the average electrical symbol power of the signal to be transmitted. The term $1 + \mathcal{K}^2$ represents the increase in the electrical power of $x_{dc}(n)$ relative to $x(n)$.

Likewise, using (25), we obtain the CCDF of PAPR of the continuous PA DCO-OFDM signal as:

$$P_{c_{dc}}(y_c) = \left[1 - \exp\left(- \frac{U_p N}{\sqrt{3}} e^{-\left(\sqrt{y_c(1+\mathcal{K}^2)} - \mathcal{K} \right)^2/2} \right) \right]^P. \tag{28}$$

When $\mathcal{B} = 0$, (27) and (28) reduces to (23) and (25) respectively. Next is the derivation of the required $\mathcal{B}$ in the PA DCO-OFDM signal.

The performance of DCO-OFDM system depends on the choice of $\mathcal{B}$. Optimum bias point is important in order to accommodate the full amplitude swings of the DCO-OFDM signal within the limited dynamic range of the LED. Thus, to avoid lower-level clipping, the condition of $\mathcal{B} \geq \mathcal{L}$ must be met, where $\mathcal{L} = \left| \underset{0 \leq n \leq NL-1}{\min} x(n) \right|$. In practice, $\mathcal{B} \geq \mathcal{L}$ may result into the DCO-OFDM signal swing exceeding the dynamic linear range of the transmitter and/or $P_{s(opt)}$ limit. In addition, it makes the scheme inefficient in terms of power by increasing the optical energy to noise power spectral density, $E_{(bopt)}/N_0$, required to meet the target BER. If $\mathcal{B}$ is not to be excessive, clipping to condition the signal to fit the optical power constraints occurs. The consequence includes distortion of the DCO-OFDM signal to be transmitted due to clipping noise [40]. However, application of peak reduction techniques in DCO-OFDM helps in reducing the required $\mathcal{B}$. In this work, $\mathcal{B}$ is modeled based on the *lower* PAPR $(\mathcal{L}^2/\sigma_x^2)$ distributions of the PA O-OFDM signal $x(n)$.

4) DC-bias of PA DCO-OFDM signal: : To begin the theoretical analysis of $\mathcal{K}$, the CDF of lower PAPR of a basic O-OFDM symbol can be shown to be:

$$F(\mathcal{K}) = \left(1 - Q\left(\sqrt{\frac{\mathcal{B}^2}{\sigma_x^2}} \right) \right)^{\alpha N} = (1 - Q(\mathcal{K}))^{\alpha N}. \tag{29}$$

Again, the CDF of $\mathcal{K}$ for a PA frame is obtained using maximum order statistics and (29). Thereafter, we obtain the DC bias distributions of the PA DCO-OFDM frames that give the least lower peak after P iterations as:

$$f_{m(1)}(\mathcal{K}) = \left[1 - (1 - Q(\mathcal{K}))^{\alpha NU_p} \right]^{P-1} \times \left[\frac{\alpha P N U_p}{\sqrt{2\pi}} e^{-\mathcal{K}^2/2} (1 - Q(\mathcal{K}))^{\alpha NU_p - 1} \right]. \tag{30}$$

Equation (30) gives the distribution of sufficient $\mathcal{K} = \mathcal{L}/\sigma_x$. The random variable $\mathcal{K}$ of this distribution represents the normalized DC bias level added on an O-OFDM symbol-by-symbol basis to avoid clipping distortion. Some previous work [41]–[43] has simulated this variable-biased system for basic DCO-OFDM. For the unclipped PA DCO-OFDM signal $x_{dc}(t)$.

In practice, a fixed DC bias will be suitable for a DCO-OFDM system. We obtain fixed $\mathcal{K}$ in PA DCO-OFDM as the expected value, $E[\mathcal{K}]$, of the distributions in (30) based on the measure of central tendency of the range of $\mathcal{K}$. This results in $\mathcal{K} \leq \mathcal{L}/\sigma_x$ per PA O-OFDM symbol. This fixed $\mathcal{K}$ does not aim at completely avoiding clipping as in (30), but rather minimizes it. We define the upper and lower clipping levels as $\mathcal{C}_{c_u}$ and $\mathcal{C}_{c_l}$ respectively in order to fit the signal within

the optical power constraints of the transmitter. Hence, the PA DCO-OFDM signal to be transmitted becomes:

$$
x'_{\mathrm{dc}}(n) = \begin{cases} \mathcal{C}_{c_u} + \bar{\mathcal{B}}, & x_{\mathrm{dc}}(n) > \mathcal{C}_{c_u} + \bar{\mathcal{B}} \\ x_{\mathrm{dc}}(n), & \mathcal{C}_{c_l} + \bar{\mathcal{B}} \le x_{\mathrm{dc}}(n) \le \mathcal{C}_{c_u} + \bar{\mathcal{B}} \quad (31) \\ \mathcal{C}_{c_l} + \bar{\mathcal{B}}, & x_{\mathrm{dc}}(n) < \mathcal{C}_{c_l} + \bar{\mathcal{B}}. \end{cases}
$$

where $\bar{\mathcal{B}} = \bar{\mathcal{K}}\sigma_x$, $\mathcal{C}_{c_u} = c_u\sigma_x$, $\mathcal{C}_{c_l} = c_l\sigma_x$, c_u and c_l are unit less coefficients representing the normalized upper and lower clipping levels respectively. Thus, a fixed bias $\bar{\mathcal{K}}$ representing the expected value of (30) is obtained as:

$$
\begin{aligned}
\bar{\mathcal{K}} =&\mathrm{E}[\mathcal{K}] = \int_0^\infty \mathcal{K} f_{\mathrm{m}(1)}(\mathcal{K})\mathrm{d}(\mathcal{K}) \\
=&\frac{\alpha P N U_p}{\sqrt{2\pi}} \int_0^\infty \left\{ \left[1 - (1 - \mathrm{Q}\,(\mathcal{K}))^{\alpha N U_p} \right]^{P-1} \times \right. \\
& \left. \left[\mathcal{K} e^{-\mathcal{K}^2/2} \left(1 - \mathrm{Q}\,(\mathcal{K}) \right)^{\alpha N U_p - 1} \right] \right\} \mathrm{d}(\mathcal{K}).
\end{aligned}
\quad (32)
$$

For clipped PA DCO-OFDM signal $x'_{\mathrm{dc}}(t)$, the average optical and electrical power becomes $P_{(\mathrm{opt})} = \mathrm{E}\{x'_{\mathrm{dc}}(t)\}$ and $P_{(\mathrm{elect})} = \mathrm{E}\{x'^2_{\mathrm{dc}}(t)\}$ respectively. The closed form expression of (32) does not exist but the numerical evaluation gives a good approximation when compared with simulated values.

A means of obtaining a closed form expression of fixed $\mathcal{K}$ is by specifying the probability, $\mathrm{P}_{\mathcal{B}}$, of an IFFT output sample getting clipped below a normalized threshold bias level $\mathcal{K}^*$. First, we take the integral of (30) to obtain the CDF of the PA DCO-OFDM frame. Thereafter, the corresponding CCDF is derived as:

$$
\begin{aligned}
\mathrm{P}_{\mathcal{B}}(\mathcal{K}^*) &= \mathrm{Pr}(\mathcal{K} > \mathcal{K}^*) \\
&= \left[1 - (1 - \mathrm{Q}(\mathcal{K}^*))^{\alpha N U_p} \right]^P
\end{aligned}
\quad (33)
$$

The $\mathcal{K}^*$ is derived from (33) as:

$$
\mathcal{K}^* = \mathrm{Q}^{-1}\left(1 - \left(1 - \mathrm{P}_{\mathcal{B}}^{1/P} \right)^{1/(\alpha N U_p)} \right). \quad (34)
$$

The closed form expression in (34) is capable of generating the normalized DC bias level based on N, U_P, P and the value of $\mathrm{P}_{\mathcal{B}}$ chosen. The fixed normalized threshold DC bias level obtained via theoretical expression in (32) and (34) at $\mathrm{P}_{\mathcal{B}} = 0.5$ is 10.3 dB and 10.4 dB respectively using $N = 256$, $U = 5$ and $P = 5$. It can be observed that there is close match between these values.

D. Signal Distribution of the ACO-OFDM frame with PA PAPR Reduction

The theoretical analysis of PAPR distributions in ACO-OFDM is presented in this section. We derive the approximate CDF of PAPR of a basic ACO-OFDM symbol with half-Gaussian distribution. Using order statistics and following the summarized procedure from Section IV-B, we obtain the analysis of PAPR distributions of ACO-OFDM. The CDF of $x_{\mathrm{aco}}(n)$ is obtained as:

$$
\begin{aligned}
\mathrm{Pr}\left(\frac{x^2_{\mathrm{aco}}(n)}{\sigma_x^2/2} \le y \right) &= \mathrm{Pr}\left(x_{\mathrm{aco}}(n) \le \sigma_x \sqrt{\frac{y}{2}} \right) \\
&= 1 - \mathrm{Q}\left(\sqrt{\frac{y}{2}} \right)
\end{aligned}
\quad (35)
$$

Using (35), the CDF of the PAPR of an L-times oversampled ACO-OFDM symbol can be approximated as:

$$
\begin{aligned}
\mathrm{Pr}(\mathrm{PAPR}_A \le y) &= \prod_{n=0}^{NL-1} \mathrm{Pr}\left(\frac{x^2_{\mathrm{aco}}(n)}{\sigma_x^2/2} \le y \right) \\
&= \left(1 - \mathrm{Q}\left(\sqrt{\frac{y}{2}} \right) \right)^{\alpha N}
\end{aligned}
\quad (36)
$$

Again, using order statistics and the summarized procedure we obtain the CCDF of PAPR of the PA ACO-OFDM signal after P iterations as:

$$
\mathrm{Pr}(\mathrm{PAPR}_A \ge y) = \left(1 - \left(1 - \mathrm{Q}\left(\sqrt{\frac{y}{2}} \right) \right)^{\alpha N} \right)^P \quad (37)
$$

In Fig. 3, we show the peak reduction capabilities of the PA ACO-OFDM with $U = 5$, $P = 5$, $\alpha = 2.8$ and $n_{\mathrm{s}} = 127$. The analytical PAPR CCDF of ACO-OFDM is presented in order to show the accuracy of the theoretical expression in (37). This figure also depicts the basic CCDF of PAPR for comparison. Results illustrating the peak reduction capability of PA technique show that 1 out of every 10^3 ACO-OFDM frames has its PAPR greater than 17.1 dB. However, the PA technique is capable of minimizing this threshold value such that 1 frame has its PAPR greater than 14.9 dB out of every 10^3 frames. This implies a PAPR reduction gain of about 2.2 dB at CCDF of 10^{-3}. Comparing the PAPR CCDF of ACO-OFDM, results show a meager difference between the results obtained via simulations and those of the theoretical expression presented in (37). This difference is also attributed to the assumption of the time domain ACO-OFDM signal distributions being perfectly half-Gaussian in analysis. Therefore, simulation results confirm the derived analytical expression of the PA ACO-OFDM technique. Fig. 3 is the CCDF plot of analytical and simulated basic and PA ACO-OFDM signal.

V. PERFORMANCE OF THE PA TECHNIQUE IN O-OFDM SYSTEM

The BER against electrical energy to noise power spectral density, $E_{\mathrm{b(elect)}}/N_0$, depends on the electrical signal-to-noise ratio (SNR) per bit, whereas the limiting factor in some IM/DD OWC systems is the average optical power that can be transmitted. Some previous studies [14], [44] have studied the performance comparison of basic O-OFDM in terms of normalized $E_{\mathrm{b(opt)}}/N_0$ and normalized bandwidth/bit rate or bit rate/normalized bandwidth in order to account for the limiting factor. Following [44], the study of the performance of PA DCO-OFDM and ACO-OFDM using the $E_{\mathrm{b(opt)}}/N_0$ and bit rate/normalized bandwidth is presented. Bandwidth is defined as the position of the first spectral null and normalized relative to the OOK with the same data rate [28]. This point of first null occur at the normalized frequency of $1 + 2/N$ in DCO-OFDM, resulting into a bit rate/normalized bandwidth of $\log_2 M/(1 + 2/N)$. In ACO-OFDM, the point of first null occur at the normalized frequency of $2(1 + 2/N)$ and the bit rate/normalized bandwidth is $\log_2 M/(2 + 4/N)$, where M is the constellation order in both cases [44]. Activating odd subcarriers only in ACO-OFDM reduces its spectral efficiency
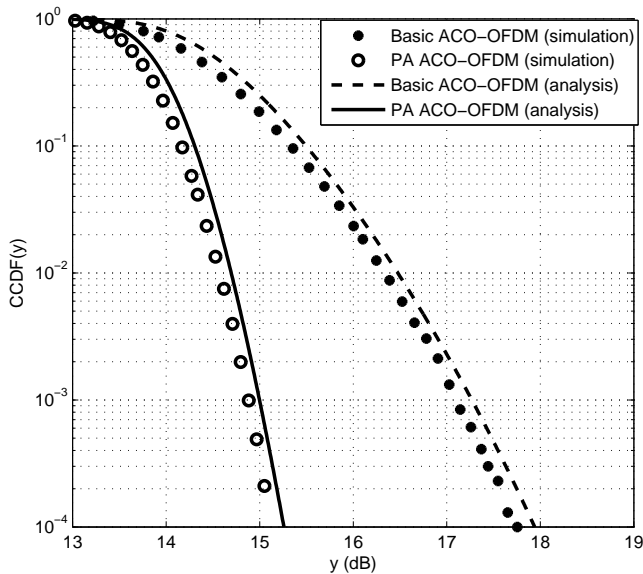
Fig. 3: CCDF plot of analytical and simulated basic and PA ACO-OFDM signal $P = 5$, $U = 5$, $n_s = 127$ and $N = 508$

when compared with DCO-OFDM for the same modulation order. As such, maintaining equivalent data rate requires M^2-QAM ACO-OFDM to be compared with M-QAM DCO-OFDM [14]. To relate $E_{b(opt)}$ to $E_{b(elect)}$, the normalized optical-to-electrical conversion ratio in DCO-OFDM and ACO-OFDM is defined as [14]:

$$\frac{E_{b(opt)}}{N_0} = \frac{E\{x'_{dc}\}^2}{E\{x'^2_{dc}\}} \frac{E_{b(elect)}}{N_0},$$ (38)

and

$$\frac{E_{b(opt)}}{N_0} = \frac{1}{\pi} \frac{E_{b(elect)}}{N_0}$$ (39)

respectively.

VI. RESULTS AND DISCUSSIONS

In this paper, basic O-OFDM represents signal with dummy pilot signal for fair comparison but no PAPR reduction technique implemented. On the other hand, PA O-OFDM involves use of pilot symbol phase to rotate data symbol phase in order to achieve PAPR reduction.

The effect of P on the reduction capability of the PA technique is studied. An expression for the reduction in PAPR for O-OFDM is obtained as follows: the threshold PAPR can be obtained from (23) and it is given by (40):

$$y^{(P)} = \left[Q^{-1}\left(\frac{1 - \left(1 - P_d^{1/P}\right)^{1/\alpha NU_p}}{2} \right) \right]^2.$$ (40)

Hence, the PAPR reduction gain in decibels (dB) can be evaluated from (40) as:

$$\text{PAPR}_{gain}(\text{dB}) = y^{(0)}(\text{dB}) - y^{(P)}(\text{dB})$$

$$= 10\log_{10}\left[\left(Q^{-1}\left(\frac{1 - (1 - P_d)^{1/\alpha NU_p}}{2} \right) \right)^2 \right.$$

$$\left. - \left(Q^{-1}\left(\frac{1 - \left(1 - P_d^{1/P}\right)^{1/\alpha NU_p}}{2} \right) \right)^2 \right]$$ (41)

where $y^{(0)}$ represents the threshold PAPR of basic O-OFDM signal. Fig. 4 shows the PAPR reduction gain in decibel for different number of pilot iterations at CCDF $= 10^{-3}$ and 10^{-4}. This plot would have been extremely difficult and time consuming to generate via computer simulations. The results in Fig. 4 show that greater PAPR reduction is achieved at lower CCDF, and as the number of iteration is increased. At CCDF $= 10^{-3}$ with $P = 100$, the gain is about 4 dB whereas it is approximately 2.5 dB at $P = 5$. These results imply that 62% of the PAPR reduction gain achieved at $P = 100$ is attainable at $P = 5$. Also, by increasing P further results only in additional little reduction in PAPR which can be described as a form of saturation effect. Since the complexity of the PA O-OFDM technique increases with increased P, value of P that gives PAPR reduction at reasonable level of complexity is important.
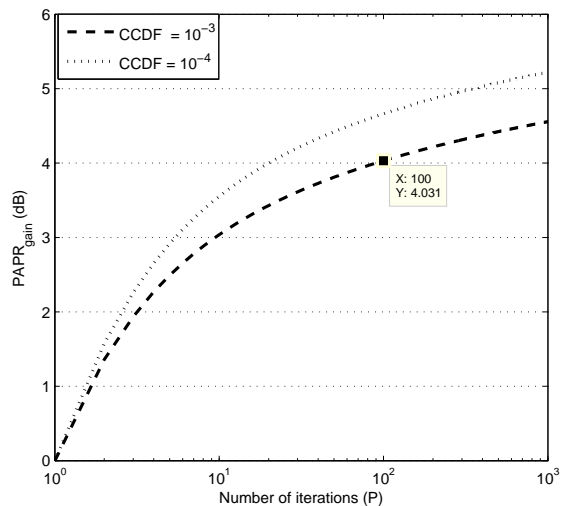

Fig. 4: PAPR reduction gain based on (41) at CCDF of 10^{-3} and 10^{-4} using $U = 5$ and $N = 256$.

Moreover, we investigate the effect of number of subcarriers on the PA PAPR reduction technique. Fig. 5 shows the plot of threshold PAPR at CCDF $= 10^{-4}$ against a wide range of N. These results based on (40) show the low sensitivity of O-OFDM signal to excessively high PAPR as the number of subcarriers more likely to add up coherently increases. At CCDF $= 10^{-4}$, increasing the number of subcarriers from $N = 512$ to $N = 1024$ yields PAPR increase of approximately 0.2 dB in basic O-OFDM. Also, by increasing N further to

2048 results in about additional 0.2 dB increase in PAPR. For the PA O-OFDM the corresponding PAPR increase is about 0.4 and 0.3 dB respectively. Although PA O-OFDM system achieves PAPR reduction for various number of subcarriers, the PAPR reduction gain reduces as N increases. Increasing N simply increases the probability of having more sinusoids that can coherently add up to produce high signal peaks at different points in time. Implementing the PA technique to rotate the phase of the subcarriers leads to a random reduction of these high peaks. As N increases, the capability of the PA technique to randomly reduce all these high signal peaks reduces. Hence, the decrease in PAPR reduction gains of the PA technique when N increases.
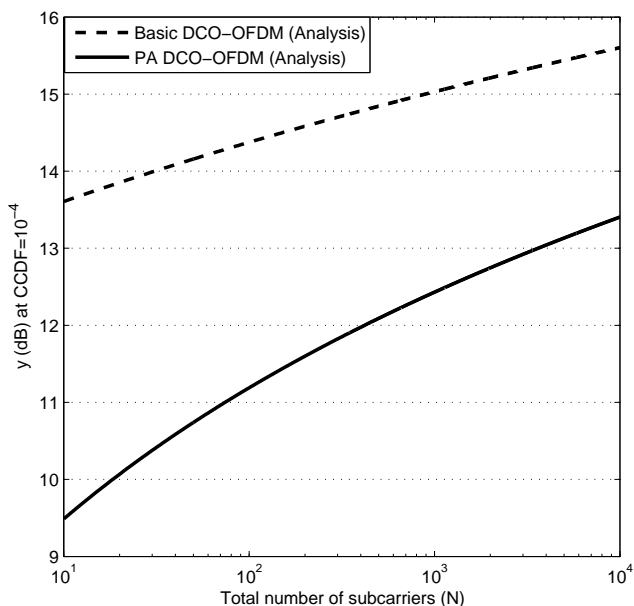

Fig. 5: PAPR threshold values based on (40) to attain a CCDF of 10^{-4} against N for basic and PA DCO-OFDM signal with $U = 5$, and $P = 5$.

Fig. 6 shows the plot of BER against $E_{b(\text{elect})}/N_0$ for different QAM constellations systems. The levels of the LED are set to $c_u = 2.7$ and $c_l = -3.2$ for the purpose of illustrating the clipping distortion minimization capability of the PA technique. Comparison between the basic and PA DCO-OFDM suggests that higher order QAM modulation in basic DCO-OFDM is more susceptible to signal clipping distortion. This is because the PA technique reduces the peaks and $\mathcal{K}$ to values less than that of basic O-OFDM. As a result, the average electrical power of the transmit signal is also minimized when the bias power is included in the calculation of the $E_{b(\text{elect})}/N_0$. In addition, as a result of mild signal clipping the Gaussian assumption is no longer true for $\mathbf{x}'_{\text{dc}}$. The clipping generates distortion on all subcarriers and there is adding of clipping noise. Thus, it is expected that the PA DCO-OFDM system gives a better BER performance than the basic counterpart under the same upper and lower clipping conditions. Results show that the basic DCO-OFDM requires more $E_{b(\text{elect})}/N_0$ to achieve target BER than PA DCO-
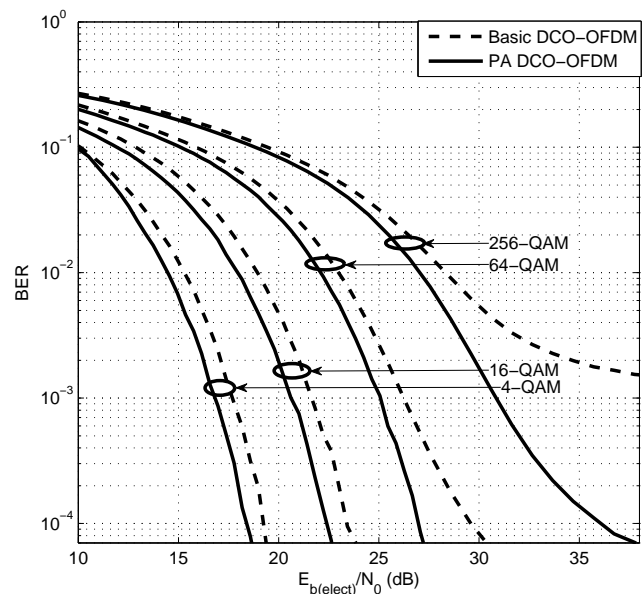

Fig. 6: BER performance for basic and PA DCO-OFDM signal with $U = 5$, $P = 5$, $N = 256$, and $[4, 16, 64, 256]$-QAM

OFDM for all the QAM systems shown. The PA DCO-OFDM has about 1 dB $E_{b(\text{elect})}/N_0$ gain for 4-, 16- and 64-QAM systems at BER $= 10^{-3}$. It is shown that basic DCO-OFDM suffers a greater BER degradation for 256-QAM system. It is unable to achieve this target BER of 10^{-3} because it has an error floor of about 2×10^{-3}.

The average optical power reduction in PA O-OFDM with the presence of signal clipping distortion and AWGN is assessed in terms of normalized $E_{b(\text{opt})}/N_0$ and bit rate/normalized bandwidth in Fig. 7. The optical power efficiency of the PA DCO-OFDM and ACO-OFDM is also compared in this figure. For this purpose, the normalized O/E conversion ratio in (38) and (39) is employed for BER $= 10^{-3}$. Focusing on the reduction achieved in $E_{b(\text{opt})}/N_0$ when PA technique is implemented in DCO-OFDM, the PA technique is capable of reducing the $E_{b(\text{opt})}/N_0$ by about 1 dB at a BER of 10^{-3} with $P = 5$. This is equivalent to about 21% reduction. The ACO-OFDM is expected to deliver a better BER performance for lower constellation order. This means the ACO-OFDM signal is still more suitable for systems requiring low average optical power while the DC bias in DCO-OFDM is also an added advantage in applications where illumination is the primary purpose of the optical source. The bit rate/normalized bandwidth value for 256-QAM basic DCO-OFDM does not exist at BER of 10^{-3} due to the error floor at about 2×10^{-3} as shown in Fig. 6. This implies that implementing the PA technique in O-OFDM provides the opportunity of conditioning the signal to meet desired system requirement.

A common feature in OFDM is the insertion of a pilot signal for synchronization and channel estimation at the receiver. However, the density of pilots used differ from one system to another. To investigate the penalty of pilot symbol pattern used
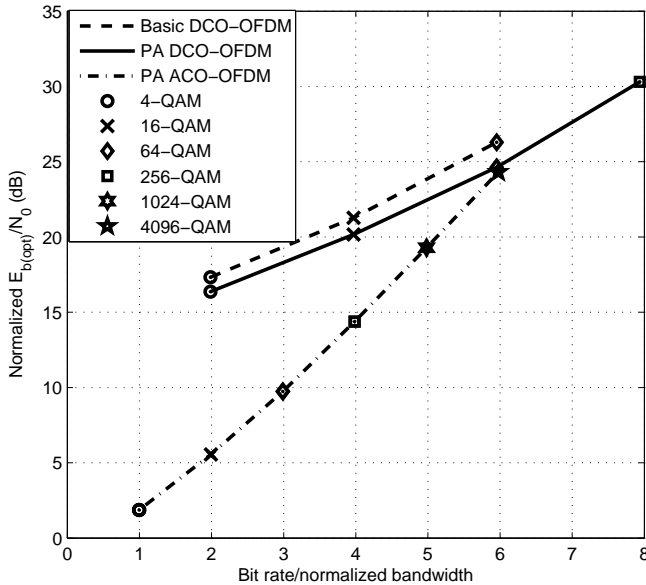
Fig. 7: $E_{b(opt)}/N_0$ against bit rate/normalized bandwidth for basic DCO-OFDM, PA DCO-OFDM and ACO-OFDM signal with $U = 5$, $P = 5$, $n_s = 127$, BER $= 10^{-3}$ and $[4, 16, 64, 256, 1024, 4096]$-QAM.
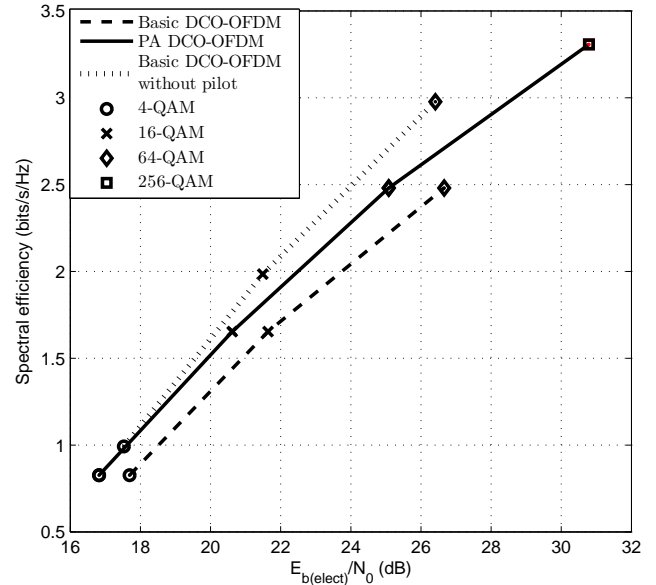

Fig. 8: Spectral efficiency against $E_{b(elect)}/N_0$ for PA DCO-OFDM, basic DCO-OFDM with and without pilot symbol using $U = 5$, $P = 5$, $N = 256$, BER $= 10^{-3}$, $[4, 16, 64, 256]$-QAM.

in the PA DCO-OFDM system, we plot the spectral efficiency against the $E_{b(elect)}/N_0$ to achieve BER of 10^{-3} in Fig. 8. Results in Fig. 8 are that of PA DCO-OFDM, basic DCO-OFDM with and without pilot symbol for fair comparison. Comparing the PA DCO-OFDM and basic DCO-OFDM without pilot symbol, there is $E_{b(elect)}/N_0$ gain of about 0.7 dB, 0.9 dB and 1.4 dB for $[4, 16, 64]$-QAM respectively when the PA technique is used. However, results show that the spectral efficiency of the PA technique decreases as the M-QAM order increases.

VII. CONCLUSIONS

In this paper, the theoretical characterization of PAPR reduction in PA DCO-OFDM and ACO-OFDM systems is presented using order statistics. To the best of our knowledge, this is the first time order statistics is utilized in the field of OWC. A comparison with simulation results is carried out to verify the accuracy of the analysis. The PA technique uses P iterations of the pilot sequence to rotate the phase of U data symbols within the O-OFDM frame. We have derived closed form expressions which give fast computation of the PAPR distributions of the PA DCO-OFDM and DCO-OFDM signal as a function of P, U_p, N, and DC bias. Since the complexity of the PA O-OFDM technique increases with increased P, value of P that gives good PAPR reduction at a reasonable level of complexity is important. As such, at CCDF $= 10^{-3}$ the analytical result in DCO-OFDM indicates that 62% of the PAPR reduction gain achieved at $P = 100$ is attainable at $P = 5$. There is also an indication of a form of saturation effect on PAPR reduction gain as P increases. This means that greater reduction is attainable as P increases but at expense of increased system

complexity. The investigation of the impact of N on PA DCO-OFDM technique depicts that PAPR reduction achievable is up to about 3 dB at CCDF $= 10^{-4}$ for $N = 256$. Results from closed form expressions also show that PAPR reduction gain increases when N decreases or when P is increased. Comparisons of the theoretical results of DC bias in DCO-OFDM signal with that of computer simulations show a very good agreement. For BER of 10^{-3} in an AWGN channel, the PA reduction technique is capable of reducing the required $E_{b(opt)}/N_0$ by about 1 dB when compared with basic DCO-OFDM where no PAPR reduction technique is implemented. The basic DCO-OFDM with 256-QAM is unable to achieve the target BER of 1×10^{-3} because it has an error floor of about 3×10^{-3}.

APPENDIX A

In this appendix, we give derivation of the distribution of the PA O-OFDM frame using (19). To accomplish this using order statistics, we find the distribution of maximum order statistics of the U_p peak distributions. Thus, the PDF of a PA O-OFDM frame is:

$$f_{Y_{(U_p)}}(y) = U_p \left[F_Y(y)\right]^{U_p-1} \frac{\mathrm{d}}{\mathrm{d}y} F_Y(y)$$

$$= U_p \left[(1 - 2Q(\sqrt{y}))^{\alpha N}\right]^{U_p-1} \frac{\mathrm{d}}{\mathrm{d}y} \left[(1 - 2Q(\sqrt{y}))^{\alpha N}\right]$$

$$= U_p \left[(1 - 2Q(\sqrt{y}))^{\alpha N}\right]^{U_p-1}$$

$$\left[\frac{\alpha N}{\sqrt{2\pi y}} e^{-y/2} \left(1 - 2Q(\sqrt{y})\right)^{\alpha N-1}\right]$$

$$\tag{A.42}$$

The corresponding CDF of a PA O-OFDM frame is obtained from (A.42) as:

$$
\begin{aligned}
F_{Y_{(U_p)}}(y) &= \int_0^y f_{Y_{(U_p)}}(t)\,\mathrm{d}t \\
&\overset{(A.42)}{=} \left[(1 - 2Q(\sqrt{t}))^{\alpha N} \right]^{U_p} \Big|_0^y \\
&= \left[(1 - 2Q(\sqrt{y}))^{\alpha N} \right]^{U_p} - \left[(1 - 2Q(\sqrt{0}))^{\alpha N} \right]^{U_p} \\
&= (1 - 2Q(\sqrt{y}))^{\alpha N U_p}.
\end{aligned}
\tag{A.43}
$$

APPENDIX B

Having obtained the distribution of the PA O-OFDM frame, here we are interested in selecting the PA O-OFDM frame that gives the minimum PAPR after P iterations. Using order statistics with the assumption that the ensemble contains P PAPR distributions, the distribution of interest corresponds to that of minimum order statistics. Therefore, the PDF of the minimum PAPR is obtained from (A.43) as:

$$
\begin{aligned}
f_{Y_{m(1)}}(y) &= P \left[1 - F_{Y_{(U_p)}}(y) \right]^{P-1} f_{Y_{(U_p)}}(y) \\
&= P \left[1 - (1 - 2Q(\sqrt{y}))^{\alpha N U_p} \right]^{P-1} \\
&\qquad \frac{\mathrm{d}}{\mathrm{d}y} \left[(1 - 2Q(\sqrt{y}))^{\alpha N U_p} \right] \\
&= P \left[1 - (1 - 2Q(\sqrt{y}))^{\alpha N U_p} \right]^{P-1} \\
&\qquad \left[\frac{\alpha N U_P}{\sqrt{2\pi y}} e^{-y/2} \left(1 - 2Q(\sqrt{y}) \right)^{\alpha N U_p - 1} \right]
\end{aligned}
\tag{B.44}
$$

The CDF of the minimum PAPR is obtained from (B.44) as:

$$
\begin{aligned}
F_{Y_{m(1)}}(y) &= \int_0^y f_{Y_{m(1)}}(t)\,\mathrm{d}t \\
&\overset{(B.44)}{=} - \left[1 - (1 - 2Q(\sqrt{t}))^{\alpha N U_p} \right]^{P} \Big|_0^y \\
&= 1 - \left[1 - (1 - 2Q(\sqrt{y}))^{\alpha N U_p} \right]^{P}.
\end{aligned}
\tag{B.45}
$$

REFERENCES

[1] Cisco visual networking index. (2016, February) Global mobile data traffic forecast update, 2015-2020. [Online]. Available: http://www.cisco.com/c/en/us/solutions/collateral/service-provider.pdf

[2] D. Tsonev, H. Chun, S. Rajbhandari, J. McKendry, S. Videv, E. Gu, M. Haji, S. Watson, A. Kelly, G. Faulkner, M. Dawson, H. Haas, and D. O'Brien, "A 3-Gb/s Single-LED OFDM-Based Wireless VLC Link Using a Gallium Nitride LED," *IEEE Photonics Technology Letters*, vol. 26, no. 7, pp. 637–640, April 2014.

[3] Z. Ghassemlooy, W. Popoola, and S. Rajbhandari, *Optical Wireless Communications: System and Channel Modelling with MATLAB*. Boca Raton, USA: CRC Press, 2012.

[4] D. Tsonev, S. Sinanović, and H. Hass, "Complete Modeling of Nonlinear Distortion in OFDM-Based Optical Wireless Communication," *Journal of Lightwave Technology*, vol. 31, no. 18, pp. 3064–3076, September 2013.

[5] Y. Hei, J. Liu, W. Li, X. Xu, and R. T. Chen, "Branch and bound methods based tone injection schemes for PAPR reduction of DCO-OFDM visible light communications," *Optics Express*, vol. 25, no. 2, pp. 595–604, 2017.

[6] T. Mao, Z. Wang, Q. Wang, and L. Dai, "Ellipse-based DCO-OFDM for visible light communications," *Optics Communications*, vol. 360, pp. 1–6, 2016.

[7] T. Zhang, Z. Ghassemlooy, C. Ma, and S. Guo, "PAPR reduction scheme for ACO-OFDM based visible light communication systems," *Optics Communications*, vol. 383, pp. 75–80, 2017.

[8] W. O. Popoola, Z. Ghassemlooy, and B. G. Stewart, "Pilot-Assisted PAPR Reduction Technique for Optical OFDM Communication Systems," *Journal of Lightwave Technology*, vol. 32, no. 7, pp. 1374–1382, April 2014.

[9] Y. Rahmatallah and S. Mohan, "Peak-to-average power ratio reduction in OFDM systems: A survey and taxonomy," *IEEE Communications Surveys and Tutorials*, vol. 15, no. 4, pp. 1567–1592, 2013.

[10] J. G. Doblado, A. C. Oria, V. Baena-Lecuyer, P. Lopez, and D. Perez-Calderon, "Cubic metric reduction for DCO-OFDM visible light communication systems," *Journal of Lightwave Technology*, vol. 33, no. 10, pp. 1971–1978, 2015.

[11] P. Bento, J. Nunes, M. Gomes, R. Dinis, and V. Silva, "Measuring the magnitude of envelope fluctuations: Should we use the PAPR?" in *IEEE 80th Vehicular Technology Conference (VTC Fall)*, Vancouver, BC, Canada, 14–17 September 2014, pp. 1–5.

[12] S. Litsyn, *Peak power control in multicarrier communications*. Cambridge University Press, 2007.

[13] Z. Yu, R. J. Baxley, and G. T. Zhou, "Peak-to-Average Power Ratio and Illumination-to-Communication Efficiency Considerations in Visible Light OFDM System," in *IEEE International Conference on Acoustics, Speech and Signal Processing (ICASSP)*, Vancouver, BC, 26–31 May 2013, pp. 5397–5401.

[14] S. Dimitrov and H. Haas, *Principles of LED Light Communications: Towards Networked Li-Fi*. Cambridge University Press, 2015.

[15] T. Jiang, M. Guizani, H.-H. Chen, W. Xiang, and Y. Wu, "Derivation of PAPR distribution for OFDM wireless systems based on extreme value theory," *IEEE Transactions on Wireless Communications*, vol. 7, no. 4, pp. 1298–1305, 2008.

[16] S. Wei, D. L. Goeckel, and P. A. Kelly, "Convergence of the complex envelope of bandlimited OFDM signals," *IEEE Transactions on Information Theory*, vol. 56, no. 10, pp. 4893–4904, 2010.

[17] H. Yu, M. Chen, and G. Wei, "Distribution of PAR in DMT systems," *Electronics Letters*, vol. 39, no. 10, pp. 799–801, May 2003.

[18] C. Ma, H. Zhang, M. Yao, Z. Xu, and K. Cui, "Distributions of PAPR and crest factor of OFDM signals for VLC," in *IEEE Photonics Society Summer Topical Meeting Series*, Seattle, USA, 9–11 July 2012, pp. 119–120.

[19] B. G. Stewart, S. G. McMeekin, and P. Liu, "Telecommunications method and system," US Patent 20 110 286 537A1, 2011.

[20] B. G. Stewart, "Telecommunications method and system," US Patent 8 126 075, February 28, 2012.

[21] F. Ogunkoya, W. Popoola, A. Shahrabi, , and S. Sinanović, "Performance Evaluation of Pilot-assisted PAPR Reduction Technique in Optical OFDM Systems," *IEEE Photonics Technology Letters*, vol. 27, no. 10, pp. 1088–1091, 2015.

[22] H. Dong, H. Zhang, k. Lang, B. Yu, and M. Yao, "OFDM Visible Light Communication Transmitter Based on LED Array," *Chinese Optics Letters*, vol. 12, no. 5, pp. 052 301–1–4, May 10 2014.

[23] M. Mossaad, S. Hranilovic, and L. Lampe, "Visible Light Communications Using OFDM and Multiple LEDs," *IEEE Transactions on Communications*, vol. 63, no. 11, pp. 4304–4313, Nov. 2015.

[24] B. Yu, H. Zhang, L. Wei, and J. Song, "Subcarrier Grouping OFDM for Visible-Light Communication Systems," *IEEE Photonics Journal*, vol. 7, no. 5, pp. 1–12, 2015.

[25] F. B. Ogunkoya, W. O. Popoola, and S. Sinanović, "Pilot-assisted PAPR Reduction Technique for O-OFDM Using Multiple LEDs in VLC Systems," in *IEEE International Conference on Communications (ICC) Workshop*, Kuala Lumpur, Malaysia, May 23–27, 2016, pp. 274–279.

[26] M. Beko and R. Dinis, "Systematic method for designing constellations for intensity-modulated optical systems," *Journal of Optical Communications and Networking*, vol. 6, no. 5, pp. 449–458, 2014.

[27] J. Grubor, V. Jungnickel, and K.-D. Langer, "Adaptive optical wireless OFDM system with controlled asymmetric clipping," in *Forty-First Asilomar Conference on Signals, Systems and Computers (ACSSC)*, 2007, pp. 1896–1902.

[28] J. M. Kahn and J. R. Barry, "Wireless Infrared Communications," *Proceedings of the IEEE*, vol. 85, no. 2, pp. 265–298, Feb. 1997.

[29] J. Armstrong and A. Lowery, "Power Efficient Optical OFDM," *Electronronics Letters*, vol. 42, no. 6, pp. 370–372, March 2006.

[30] S. Lee, S. Randel, F. Breyer, and A. Koonen, "PAM-DMT for Intensity-Modulated and Direct-Detection Optical Communication Systems," *IEEE Photonics Technology Letters*, vol. 21, no. 23, pp. 1749–1751, December 2009.

[31] D. Tsonev, S. Sinanović, and H. Haas, "Novel Unipolar Orthogonal Frequency Division Multiplexing (U-OFDM) for Optical Wireless," in *75th IEEE Vehicular Technology Conference (VTC Spring)*, Yokohama, 6–9 May 2012, pp. 1–5.

[32] D. Tsonev, S. Videv, and H. Haas, "Unlocking spectral efficiency in intensity modulation and direct detection systems," *IEEE Journal on Selected Areas in Communications*, vol. 33, no. 9, pp. 1758–1770, 2015.

[33] H. Elgala and T. Little, "P-OFDM: Spectrally efficient unipolar OFDM," in *Optical Fiber Communication Conference and Exhibition (OFC)*, San Francisco, CA, 9–13 March 2014, pp. 1–3.

[34] G. Casella and R. L. Berger, *Statistical Inference*, 2nd ed. Duxbury, 2002.

[35] H.-C. Yang and M.-S. Alouini, *Order statistics in wireless communications: diversity, adaptation, and scheduling in MIMO and OFDM systems*. Cambridge University Press, 2011.

[36] N. Balakrishnan and C. R. Rao, *Order statistics: applications*. Amsterdam: Elsevier, 1998.

[37] K. Wong, M.-O. Pun, and H. Poor, "The Continuous-Time Peak-to-Average Power Ratio of OFDM Signals Using Complex Modulation Schemes," *IEEE Transactions on Communications*, vol. 56, no. 9, pp. 1390–1393, September 2008.

[38] Z. Yu, R. J. Baxley, and G. T. Zhou, "Iterative Clipping for PAPR Reduction in Visible Light OFDM Communication," in *IEEE Military Communication Conference (MILCOM)*, Baltimore, MD, 6–8 October 2014, pp. 1681–1686.

[39] R. van Nee and A. de Wild, "Reducing the peak-to-average power ratio of OFDM," in *48th IEEE Vehicular Technology Conference (VTC)*, Ottawa, 18–21 May 1998, pp. 2072–2076.

[40] S. Dimitrov, S. Sinanović, and H. Haas, "Clipping Noise in OFDM-Based Optical Wireless Communication Systems," *IEEE Transactions on Communications*, vol. 60, no. 4, pp. 1072–1081, April 2012.

[41] L. Chen, B. Krongold, and J. Evans, "Performance Analysis for Optical OFDM Transmission in Short-range IM/DD Systems," *Journal of Lightwave Technology*, vol. 30, no. 7, pp. 974–983, April 2012.

[42] W. Kang and S. Hranilovic, "Power reduction techniques for multiple-subcarrier modulated diffuse wireless optical channels," *IEEE Transactions on Communications*, vol. 56, no. 2, pp. 279–288, February 2008.

[43] L. Chen, B. Krongold, and J. Evans, "Theoretical characterization of nonlinear clipping effects in IM/DD optical OFDM systems," *IEEE Transactions on Communications*, vol. 60, no. 8, pp. 2304–2312, August 2012.

[44] S. D. Dissanayake and J. Armstrong, "Comparison of ACO-OFDM, DCO-OFDM and ADO-OFDM in IM/DD Systems," *Journal of Lightwave Technology*, vol. 31, no. 7, pp. 1063–1072, April 2013.